

Optimal Temporal Patterns for Dynamical Cellular Signaling

Yoshihiko Hasegawa

March 26, 2022

Department of Information and Communication Engineering, Graduate School of Information Science and Technology, The University of Tokyo, Tokyo 113-8656, Japan

Abstract

Cells use temporal dynamical patterns to transmit information via signaling pathways. As optimality with respect to the environment plays a fundamental role in biological systems, organisms have evolved optimal ways to transmit information. Here, we use optimal control theory to obtain the dynamical signal patterns for the optimal transmission of information, in terms of efficiency (low energy) and reliability (low uncertainty). Adopting an activation-deactivation decoding network, we reproduce several dynamical patterns found in actual signals, such as steep, gradual, and overshooting dynamics. Notably, when minimizing the energy of the input signal, the optimal signals exhibit overshooting, which is a biphasic pattern with transient and steady phases; this pattern is prevalent in actual dynamical patterns. We also identify conditions in which these three patterns (steep, gradual, and overshooting) confer advantages. Our study shows that cellular signal transduction is governed by the principle of minimizing free energy dissipation and uncertainty; these constraints serve as selective pressures when designing dynamical signaling patterns.

1 Introduction

Cells transmit information through signal transduction and transcription networks [1,2]. Recent studies have revealed that, along with the identity and static concentration of molecules, cells also encode information into dynamical patterns [3–9]. Examples of dynamical patterns include extracellular signal-regulated kinase (ERK), the yeast transcription factor Msn2, the transcription factor NF- κ B, a protein kinase AKT, and calcium signaling. Many studies have used nonlinear and stochastic approaches to investigate the properties of dynamical cellular information processing [10–17]. Because signal transduction plays central and crucial roles in the survival of cells, the time course of dynamical patterns is expected to be highly optimized so that cells can efficiently and accurately transmit information. Although the advantages of dynamical signals over static ones have been extensively studied [8,18], there has been little investigation into determining which dynamical signals are the best. We assume that two principles that are prevalent in many biological systems govern the optimality of signal patterns: energetic efficiency (low energy) and reliability (low uncertainty). Biological systems are often characterized by low energy consumption. For instance, neuronal systems are known to function with remarkably low energy consumption. Specifically, in neurons, information processing capability is bounded by the amount of energy consumption and it is reported that the energy consumption of the brain has limited its size ([19,20] and references therein). Biochemical networks process information for a variety of purposes, and higher specificity, lower variation, and larger signal amplification demand more energy consumption [21]. These facts induce us to think that the energetic cost also plays important roles in information transmission of the dynamical signal transduction. A major cause of interference with reliability is molecular noise, which degrades the quality of transmitted information. Despite the stochastic nature of cellular processes, organisms have acquired several mechanisms to resist or to take advantage of noise in order to enhance biological functionalities [22]. As these two principles are of significance, the dynamical transmission of information has evolved in such a way that it optimally satisfies these principles. We divide the dynamical signal transduction into two parts: encoding of extracellular stimuli into intracellular dynamical patterns, and decoding of the dynamical patterns into the response (in the present manuscript, the

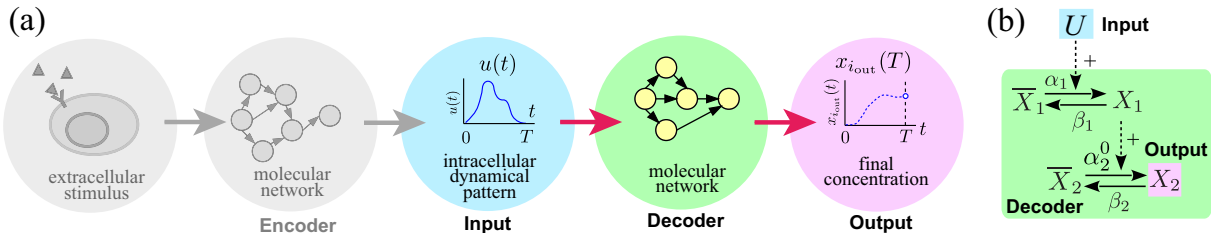


Figure 1: Overview of dynamical signal transduction. (a) An extracellular stimulus is encoded into an intracellular dynamical pattern. The decoder reads the dynamical pattern and outputs the result as the final concentration. This study focuses on the latter process (colored flow). The intracellular dynamical pattern $u(t)$ and the final concentration $x_{i_{out}}(T)$ correspond to input and output, respectively, and we optimize the dynamical pattern. (b) Two-molecule decoding network (the two-stage model), which reports the result as X_2 . \bar{X}_i and X_i ($i = 1, 2$) denote the inactive and active molecules, respectively.

response corresponds to the concentration of output molecular species) (Fig. 1(a)). By viewing the dynamical signal as an input, the decoding network as the system to be controlled, and the output concentration as an output (Fig. 1(a)), we use optimal control theory [23,24] to determine the signal dynamics that optimize energy efficiency and the reliability of transmitted information. We quantify the energetic cost by free energy dissipation when generating temporal dynamical patterns and the uncertainty by variance of output molecular species concentration. To decode the dynamical signals, we adopt an activation-deactivation network (Fig. 1(b)), which is a motif commonly used in biochemical networks. We optimize the dynamical patterns, i.e. the input. Decoders (decoding networks) may also coevolve to maximally reading out information from signals, but in this paper, we focus on optimizing the input. No matter how precisely the decoder is able to read dynamical signals, it is impossible to totally eliminate the uncertainty due to the inherent stochasticity. Therefore, there is a lower bound on the uncertainty and the bound is determined by input.

From our calculations, we identify three basic patterns for the signals: steep (Fig. 2(a)), gradual (Fig. 2(b)), and overshooting (Fig. 2(c)). We show that the steep pattern minimizes the energy, whereas the gradual pattern minimizes the uncertainty. Intriguingly, when minimizing the energy of a dynamical pattern while achieving a higher output concentration, overshooting is the optimal pattern; this pattern can often be seen in real processes. We identify the conditions in which these three patterns (steep, gradual, and overshooting) confer advantages. We note that these patterns are prevalent in signal transduction, and our calculations show that minimizing the energetic cost and uncertainty plays important roles in the evolutionary design of dynamical signaling patterns.

2 Methods

2.1 Model

Dynamical signal transduction is typically separated into two parts [7]: encoding of extracellular stimuli into intracellular dynamical patterns, and decoding of the dynamical patterns into the response (Fig. 1(a)); our study focuses on the latter process, and dynamical signals are optimized for readout by a particular decoder, where the optimization criteria are to minimize the energy consumed by signal generation and to minimize the uncertainty of the readout.

In cells, dynamical signals are decoded by molecular networks. We consider a molecular network consisting of N molecular species X_1, X_2, \dots, X_N and we define x_i as the concentration of X_i . The input signal is carried by a molecular species U , whose concentration $u(t)$ follows a dynamic pattern, and its onset is $t = 0$. In our analysis, we use optimal control theory to optimize the temporal pattern of $u(t)$. Let the i_{out} th molecular species $X_{i_{out}}$ be the output of the network. The network reads the information from the input $u(t)$ (i.e., intracellular dynamical signal) and outputs the result as the concentration of $X_{i_{out}}$ at time T ($T > 0$) (Fig. 1(a)), i.e., $x_{i_{out}}(T)$ carries information about the input signal.

Consider the evolutionary design of the dynamical signal $u(t)$ that attains the desired concentration of an output molecule $X_{i_{out}}$ at $t = T$. Although there might be many possible dynamics for $u(t)$ ($0 \leq t \leq T$) that

result in the desired output concentration, the most biologically preferable ones are selected. We can expect that the signals with lower energetic cost will be selected. In addition, biochemical reactions are subject to noise, due to the smallness of the cells. The noise degrades the information, and hence transmission with lower uncertainty is desirable. Considering the energy of the input and the uncertainty of the concentration of the output molecule, we wish to find a signal $u(t)$ that minimizes a performance index R , defined as

$$R = \gamma_{i_{\text{out}}}(T) + w\Pi, \quad (1)$$

where $\gamma_i(t) = \langle (x_i(t) - \mu_i(t))^2 \rangle$ is the variance of the concentration of the i th molecule at time t [$\mu_i(t) = \langle x_i(t) \rangle$ is the mean] which quantifies the uncertainty, Π is the energetic cost of the signal $u(t)$, and w is a weight parameter in the range $0 < w < \infty$, which represents the importance of the energy for the performance index. As denoted, the output $X_{i_{\text{out}}}$ has the target concentration at time $t = T$. Therefore, the mean concentration of the output $X_{i_{\text{out}}}$, which we denote as $\mu_{i_{\text{out}}}(t)$, must attain the predefined target concentration $\mu_{i_{\text{out}}}^{\text{trg}}$ (“trg” is short for “target”) at time $t = T$, i.e.,

$$\mu_{i_{\text{out}}}(T) = \mu_{i_{\text{out}}}^{\text{trg}} \quad (2)$$

is a boundary condition.

2.2 Quantification of uncertainty

We quantify the uncertainty as the variance of the output molecular species concentration $\gamma_{i_{\text{out}}}(T)$; the derivation is shown below. The dynamics of molecular networks, which decode $u(t)$ and output the result, can be generally captured by the following rate equation:

$$\dot{x}_i(t) = \sum_{\ell=1}^{N_r} s_{i\ell} v_{\ell}(\mathbf{x}, u),$$

where $\mathbf{x} = (x_1, x_2, \dots, x_N)$, $\{s_{i\ell}\} = \mathbf{S}$ is a stoichiometry matrix, $v_{\ell}(\mathbf{x}, u)$ is the reaction velocity of the ℓ th reaction, and N_r is the number of reactions. Due to the smallness of the cells, chemical reactions are subject to stochasticity. We describe the noisy dynamics by the Fokker–Planck equation (FPE) [25, 26]:

$$\frac{\partial}{\partial t} P(\mathbf{x}; t) = - \sum_i \frac{\partial}{\partial x_i} \sum_{\ell} s_{i\ell} v_{\ell}(\mathbf{x}, u) P(\mathbf{x}; t) + Q \sum_{i,j} \frac{\partial^2}{\partial x_i \partial x_j} \sum_{\ell} s_{i\ell} s_{j\ell} v_{\ell}(\mathbf{x}, u) P(\mathbf{x}; t), \quad (3)$$

where $P(\mathbf{x}; t)$ is the probability density of \mathbf{x} at time t , and Q is the noise intensity related to the volume V via $Q = (2V)^{-1}$. Optimal control theory and related variational methods have been employed by many researchers [27–31]. Although stochastic optimal control theory has been applied in biological contexts [31], it is difficult to apply it to multivariate models. Instead, we describe the dynamics by using the time evolution of moments derived from Eq. (3) [32, 33]. For general nonlinear models, the naive calculation of moment equations results in an infinite hierarchy of differential equations. Because our adopted models are linear with respect to \mathbf{x} (cf. Eqs. (15) and (16)), we can obtain closed differential equations (see the supplementary material). For moments of up to the second order [mean $\mu_i(t)$, variance $\gamma_i(t)$, and covariance $\rho_{ij} = \langle (x_i - \mu_i)(x_j - \mu_j) \rangle$], we have the following moment equation with respect to $\mathbf{z} = (\mu_1, \dots, \mu_n, \gamma_1, \dots, \gamma_n, \rho_{12}, \rho_{23}, \dots, \rho_{1n})$:

$$\dot{z}_i(t) = h_i(\mathbf{z}, u), \quad (4)$$

where $h_i(\mathbf{z}, u)$ is right-hand side of the moment equation and the dimensionality of \mathbf{z} is $M = N(N + 3)/2$. With the moment equation (4), we can reduce the stochastic optimal control problem to a deterministic one.

2.3 Quantification of energetic cost

We next define the energetic cost of a signal (Π in Eq. (1)) as the free energy dissipated by controlling the concentration $u(t)$ such that it follows the desired temporal dynamics. We derive the energetic cost of the

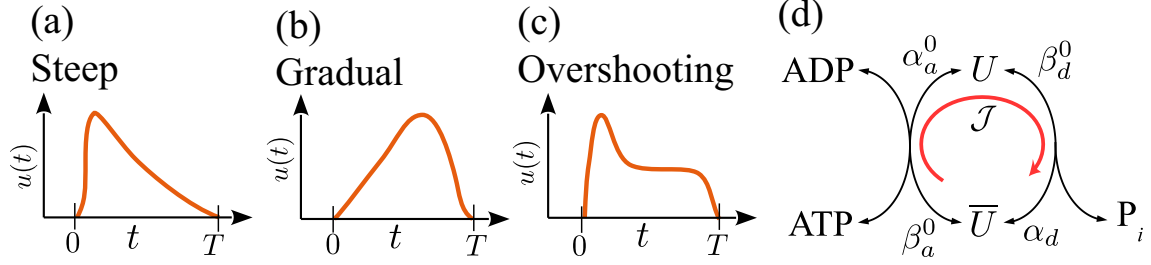
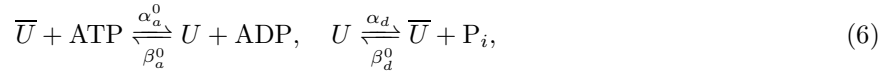


Figure 2: (a)–(c) Dynamical signal $u(t)$ ($0 \leq t \leq T$) as a function of t for the three typical patterns: (a) steep, (b) gradual, and (c) overshooting. (d) Activation-deactivation of signaling molecule U . Inactive molecule \bar{U} is activated to become active molecule U , which is mediated by phosphorylation, and deactivation is mediated by dephosphorylation. Net flux \mathcal{J} occurs in the clockwise direction (shown by an arrow).

signal U with a simple biochemical model after Ref. [34–36]. We assume that input molecular species U is activated from \bar{U} and undergoes the following reaction:



Note that the total concentration $u^{\text{tot}} = u + \bar{u}$ does not change with time, where u and \bar{u} are the concentrations of U and \bar{U} , respectively. In general, the deactivation reaction is not the reverse of activation. Therefore, when considering the energetic cost of generating U , we have to handle activation and deactivation separately. Activation is typically mediated by phosphorylation, where \bar{U} is activated by a kinase through the transfer of phosphate from ATP. The deactivation is mediated by dephosphorylation, in which a phosphatase transfers inorganic phosphate (P_i) to the solution. These reactions are written as



where α_a^0 , β_a^0 , α_d , and β_d^0 are reaction rates. When these parameters are held constant and the system is closed, the system relaxes to an equilibrium state. Let c_T , c_D , and c_P be the concentrations of ATP, ADP, and P_i , respectively. In the natural cellular environment where the system is open, c_T , c_D , and c_P can be regarded as constant, due to external agents [35], which we denote as c_T^0 , c_D^0 , and c_P^0 , respectively. Therefore the system relaxes to a nonequilibrium steady state (NESS). The steady-state concentration of U is

$$u^{\text{ss}} = \frac{u^{\text{tot}} (\beta_d + \alpha_a)}{\beta_a + \beta_d + \alpha_a + \alpha_d}, \quad (7)$$

where $\beta_a = \beta_a^0 c_D^0$, $\alpha_a = \alpha_a^0 c_T^0$, and $\beta_d = \beta_d^0 c_P^0$. At the steady state, the net flux (clockwise direction in Fig. 2(d)) is $\mathcal{J}^{\text{ss}} = u^{\text{tot}} (\alpha_a \alpha_d - \beta_a \beta_d) / (\beta_a + \beta_d + \alpha_a + \alpha_d)$. The free energy dissipated during one cycle (i.e., $\bar{U} \rightarrow U \rightarrow \bar{U}$ in the clockwise direction in Fig. 2(d)) is $\Delta\phi = k_B \mathcal{T} \ln \{ \beta_a \beta_d / (\alpha_a \alpha_d) \}$, where k_B is the Boltzmann constant and \mathcal{T} is the temperature (see the supplementary material). Therefore the instantaneous free-energy dissipation (i.e., power) is

$$\mathcal{P} = -\mathcal{J}^{\text{ss}} \Delta\phi = \frac{k_B \mathcal{T} u^{\text{tot}} (\alpha_a \alpha_d - \beta_a \beta_d)}{\beta_a + \beta_d + \alpha_a + \alpha_d} \ln \left(\frac{\alpha_a \alpha_d}{\beta_a \beta_d} \right). \quad (8)$$

Equation (8) quantifies the cost of the activation-deactivation of U . Next, in order to yield the dynamics of U , we assume that kinase activity is controlled by an upstream molecular species and thus α_a varies temporally. We assume that the relaxation of Eq. (6) is very fast [i.e., $1/(\beta_a + \beta_d + \alpha_a + \alpha_d)$ is very small] so that the concentration u is well approximated by u^{ss} (Eq. (7)) even for the case of a time-varying α_a . From Eq. (7), α_a can be represented as a function of u :

$$\alpha_a = \frac{u}{u^{\text{tot}} - u} (\alpha_d + \beta_a) - \beta_d. \quad (9)$$

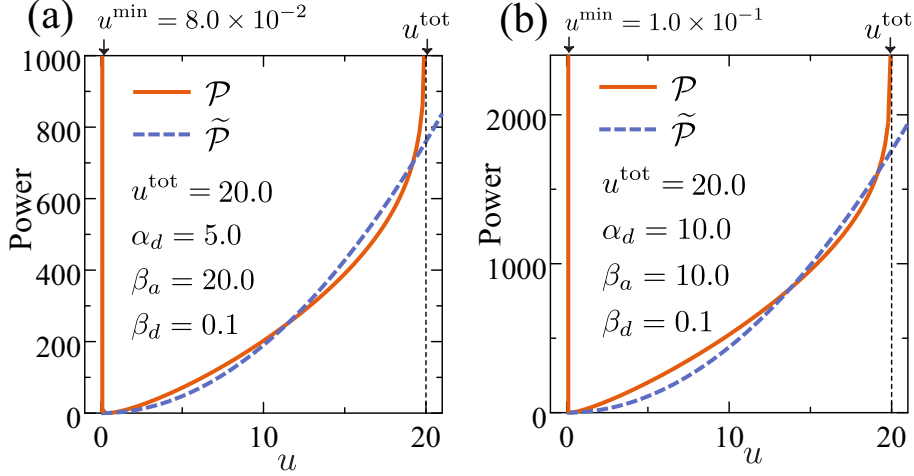


Figure 3: Exact representation of the power \mathcal{P} (solid line) and its quadratic approximation $\tilde{\mathcal{P}}$ (dashed line). (a) $u^{\text{tot}} = 20.0$, $\alpha_d = 5.0$, $\beta_a = 20.0$, and $\beta_d = 0.1$ ($q = 1.9$ for quadratic); and (b) $u^{\text{tot}} = 20.0$, $\alpha_d = 10.0$, $\beta_a = 10.0$, and $\beta_d = 0.1$ ($q = 4.4$ for quadratic). We use $k_B = 1$ and $\mathcal{T} = 1$, without loss of generality.

From the condition $\alpha_a > 0$, the minimum of u is $u^{\min} = \beta_d u^{\text{tot}} / (\beta_a + \beta_d + \alpha_d)$. For this dynamic case, the instantaneous free energy dissipation is given as a function of u which is Eq. (8) along with Eq. (9). The molecular species upstream from U also consumes energy; however, signal transduction generally amplifies the external stimuli, and so the concentration of the upstream molecular species is less than the concentration of U [37, 38]. Furthermore, we assume that the concentration of the molecular species downstream from U is also less than that of U [37, 38]. Indeed, in the ERK pathway, the concentration of ERK is higher than that of its downstream molecular species (that is, the energetic cost of decoding U is smaller than the cost of generating it). Therefore, we assume that the energetic cost of generating U (i.e., Eq. (8)) dominates the overall energetic cost. The free energy dissipated during $0 \leq t \leq T$ is

$$\Pi = \int_0^T \mathcal{P} dt. \quad (10)$$

Because it is difficult to use the exact representation of Π in the optimal control calculation, we approximate \mathcal{P} with a simpler expression: $\mathcal{P} = 0$ at a zero-flux point $u = u^{\text{zf}} = \beta_d u^{\text{tot}} / (\beta_d + \alpha_d)$ where \mathcal{J} vanishes. Assuming that u^{zf} is sufficiently small, $\mathcal{P} = 0$ when u is very low concentration. Furthermore, \mathcal{P} increases superlinearly as u increases from the zero-flux point $u = u^{\text{zf}}$. Taking into account the conditions and computational feasibility, we use the approximation $\mathcal{P} \simeq \tilde{\mathcal{P}}$ with $\tilde{\mathcal{P}} = qu^2$, where q is a proportionality coefficient. Then, the free energy dissipation during the period $0 \leq t \leq T$ is approximated by

$$\tilde{\Pi} = \int_0^T \tilde{\mathcal{P}} dt = \int_0^T qu(t)^2 dt. \quad (11)$$

Figure 3 compares the exact expression of \mathcal{P} (Eq. (8) along with Eq. (9)) with its quadratic approximation $\tilde{\mathcal{P}}$ for two settings; the exact and quadratic results are shown by solid and dashed lines, respectively. For both parameter settings, we see that the behavior of the quadratic approximation is similar to that of the exact one. The major difference between the exact and the quadratic representations is that Eq. (8) diverges to ∞ for $u \rightarrow u^{\min}$ and $u \rightarrow u^{\text{tot}}$. Therefore, in order for the quadratic expression to well approximate the exact energetic cost, u^{tot} should satisfy requirements in addition to the condition of u^{zf} . If u^{tot} is too small, the energy divergence at $u = u^{\text{tot}}$ prevents the signal to have higher peaks. On the other hand, if u^{tot} is excessively large, the exact energetic cost becomes almost linear with respect to u which makes the quadratic approximation less reliable. With this approximation, we set $u(t) = 0$ for $t < 0$ and $u(t) \geq 0$ for $t > 0$ (we define that the onset is the time when $u(t)$ becomes positive).

2.4 Finding the optimal signaling pattern

We wish to obtain the optimal control $u(t)$ that minimizes R of Eq. (1) while satisfying Eq. (4) and the predefined target mean concentration of Eq. (2) [$\mu_{i_{\text{out}}}(T) = z_{i_{\text{out}}}(T) = \mu_{i_{\text{out}}}^{\text{trg}}$]. Then, by virtue of optimal control theory [23, 24], we minimize the following augmented performance index:

$$\tilde{R} = \gamma_{i_{\text{out}}}(T) + w\tilde{\Pi} + \nu (z_{i_{\text{out}}}(T) - \mu_{i_{\text{out}}}^{\text{trg}}) + \sum_{i=1}^M \int_0^T \lambda_i (h_i(\mathbf{z}, u) - \dot{z}_i) dt, \quad (12)$$

where ν and $\boldsymbol{\lambda} = (\lambda_1, \lambda_2, \dots, \lambda_M)$ are Lagrange multipliers that force the constraints. In Eq. (12), the exact energetic cost Π in R is replaced by its quadratic approximation $\tilde{\Pi}$ (we set $q = 1$, because the scaling of q is offset by w). Using the calculus of variations [23, 24], finding an optimal signal $u(t)$ is reduced to solving the differential equations given by Eq. (4) and

$$\dot{\lambda}_i(t) = -\frac{\partial}{\partial z_i} H(\mathbf{z}, u, \boldsymbol{\lambda}), \quad (13)$$

$$0 = \frac{\partial}{\partial u} H(\mathbf{z}, u, \boldsymbol{\lambda}), \quad (14)$$

where $H(\mathbf{z}, u, \boldsymbol{\lambda})$ is the Hamiltonian [23, 24]:

$$H(\mathbf{z}, u, \boldsymbol{\lambda}) = w\tilde{\mathcal{P}} + \sum_{i=1}^M \lambda_i h_i(\mathbf{z}, u).$$

We assume vanishing initial values for all moments: $\mu_i(0) = 0$, $\gamma_i(0) = 0$, and $\rho_{ij}(0) = 0$ [i.e., $z_i(0) = 0$ for all i]. For the boundary conditions, $\lambda_{N+i_{\text{out}}}(T) = 1$ and $\lambda_i(T) = 0$ ($i \neq i_{\text{out}}, N + i_{\text{out}}$) are required from the optimal control theory, and $z_{i_{\text{out}}}(T) = \mu_{i_{\text{out}}}^{\text{trg}}$ for the final value of z_i . There are boundary conditions at both $t = 0$ and $t = T$; this two-point boundary value problem can be solved numerically by using general solvers (see the supplementary material).

3 Results

We consider the following activation-deactivation decoding motif (Fig. 1(b)): an inactive molecule \bar{X}_1 is activated to become X_1 , where the activation is dependent on the input molecule U . The rate equation is $\dot{x}_1 = \alpha_1 u (x_1^{\text{tot}} - x_1) - \beta_1 x_1$, where x_1^{tot} is the total concentration $x_1^{\text{tot}} = x_1 + \bar{x}_1$ which does not change with time (\bar{x}_1 is the concentration of \bar{X}_1), and α_1 and β_1 are activation and deactivation rates, respectively. The activated molecule X_1 activates an output molecule X_2 (e.g. an activated transcription factor), and hence X_2 reports the result (i.e., $i_{\text{out}} = 2$). The rate equation is $\dot{x}_2(t) = \alpha_2^0 x_1 (x_2^{\text{tot}} - x_2) - \beta_2 x_2$, where $x_2^{\text{tot}} = x_2 + \bar{x}_2$, and α_2^0 and β_2 are activation and deactivation rates, respectively (\bar{x}_2 is the concentration of \bar{X}_2). When x_2 is far from its saturation concentration, activation of X_2 is approximately the first-order reaction with respect to X_1 , i.e., $\dot{x}_2 = \alpha_2 x_1 - \beta_2 x_2$ where $\alpha_2 = \alpha_2^0 x_2^{\text{tot}}$. Then dynamics of X_1 and X_2 is represented by the following linear differential equation:

$$\dot{x}_1(t) = \alpha_1 u (x_1^{\text{tot}} - x_1) - \beta_1 x_1, \quad (15)$$

$$\dot{x}_2(t) = \alpha_2 x_1 - \beta_2 x_2. \quad (16)$$

Because of the linearity of Eqs. (15) and (16), the moment equation can be obtained without the truncation approximation¹. As denoted above, the input signal $u(t)$ must produce the dynamics that satisfy the constraint that the target mean concentration of X_2 at time $t = T$ is μ_2^{trg} ($i_{\text{out}} = 2$ in Eq. (2)). This type of decoding motif is prevalent and can be found in various biochemical systems [13, 39–41]. We call this a *two-stage model*. By incorporating intrinsic noise due to a small number of molecules, we have a corresponding FPE from Eq. (3) (see the supplementary material). We then calculate the moment equation from the FPE.

¹Note that linearity is not a prerequisite for applying the moment method. For nonlinear cases, closed moment equations can be obtained by truncating higher order moments than the second.

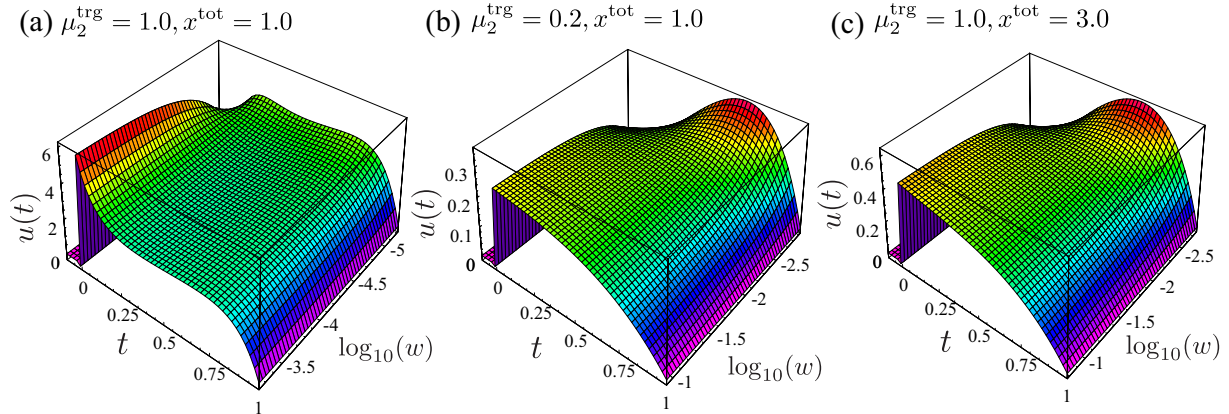


Figure 4: Optimal signal $u(t)$ for the two-stage model as a function of t and $\log_{10}(w)$ for three cases: (a) $\mu_2^{\text{trg}} = 1.0$ and $x_1^{\text{tot}} = 1.0$, (b) $\mu_2^{\text{trg}} = 0.2$ and $x_1^{\text{tot}} = 1.0$, and (c) $\mu_2^{\text{trg}} = 1.0$ and $x_1^{\text{tot}} = 3.0$. The range of w is $6.0 \times 10^{-6} \leq w \leq 6.0 \times 10^{-4}$ ($-5.22 \leq \log_{10} w \leq -3.22$) for (a), $1.2 \times 10^{-3} \leq w \leq 1.2 \times 10^{-1}$ ($-2.92 \leq \log_{10} w \leq -0.92$) for (b), and $1.7 \times 10^{-3} \leq w \leq 1.7 \times 10^{-1}$ ($-2.77 \leq \log_{10} w \leq -0.77$) for (c). The other parameters are $\alpha_1 = 2.0$, $\alpha_2 = 2.0$, $\beta_1 = 1.0$, $\beta_2 = 1.0$, $Q = 0.001$, and $T = 1.0$.

3.1 Steep pattern minimizes energetic cost, and gradual pattern minimizes uncertainty

Using the two-stage model, we calculated the optimal signal $u(t)$. Figures 4(a)–(c) shows the optimal signal $u(t)$ as a function of t and $\log_{10}(w)$ for three settings: (a) $\mu_2^{\text{trg}} = 1.0$ and $x_1^{\text{tot}} = 1.0$, (b) $\mu_2^{\text{trg}} = 0.2$ and $x_1^{\text{tot}} = 1.0$, and (c) $\mu_2^{\text{trg}} = 1.0$ and $x_1^{\text{tot}} = 3.0$. Note that $\mu_2^{\text{trg}} = 1.0$ is a near-saturation value with $x_1^{\text{tot}} = 1.0$, i.e., it is close to the maximal reachable target concentration. The other parameters are shown in the caption of Fig. 4. The minimum value for w is determined such that $u(t)$ satisfies $u(t) \geq 0$, and the maximum is 10^2 times the minimum². In all the three cases [Figs. 4(a)–(c)], for larger values of w , we see that the optimal signals steeply increase at $t = 0$ and gradually decay as time elapses. As w decreases, the optimal pattern varies from steeper to more-gradual patterns. Comparing Figs. 4(a) and (b), we can see the effect of different target concentrations. The target concentration for Fig. 4(b) is lower than it is for (a) (the other parameters are the same). For Fig. 4(a), the decay right after $t = 0$ is especially rapid, and this is followed by a plateau state ($t = 0.2$ – 0.8); this is a typical overshooting pattern, similar to that shown in Fig. 2(c). However, the optimal signal of Fig. 4(b) does not exhibit overshooting. We next compared Figs. 4(a) and (c) when all parameters are identical except for x_1^{tot} [x_1^{tot} for Fig. 4(c) is larger than it is for (a)] to see how the overshooting pattern depends on the total concentration x_1^{tot} . When the total concentration x_1^{tot} is larger, the optimal signal does not overshoot. From these results, we see that the steep pattern minimizes the energy, whereas the gradual pattern minimizes the variance. Along with the condition of the steep pattern, the overshooting pattern emerges when the target concentration μ_2^{trg} is relatively high and the total concentration x_1^{tot} is relatively low.

In Fig. 5(a), we compared the optimal signal (solid line), which exhibits the overshooting pattern, with a constant signal (dashed line), for the period starting at $t = 0$ and ending at $t = T$; both patterns attain the same target concentration $\mu_2^{\text{trg}} = 1.0$ ($w = 1.0$ for the optimal signal, which is large enough to show overshooting; the other parameters are the same as in Fig. 4(a)). Although in the interval $t = 0$ – 0.2 , the concentration of the optimal signal is larger than that of the constant signal, the optimal one yields a smaller concentration for $t > 0.2$. The energy (quadratic approximation) of the optimal signal is $\tilde{\Pi}_{\text{opt}} = 9.02$ whereas that of the constant one is $\tilde{\Pi}_{\text{const}} = 10.77$ and thus the ratio is $\tilde{\Pi}_{\text{opt}}/\tilde{\Pi}_{\text{const}} = 0.84$. We also calculated the ratio for the exact energy definition Π (parameter details are the same as in Fig. 3(a)) and we obtained $\Pi_{\text{opt}}/\Pi_{\text{const}} = 0.83^3$, where Π_{opt} and Π_{const} are defined analogously. Therefore the optimal signal obtained

²When w is below the minimal values, the signal determined by the optimal control approach violates the positivity condition at an earlier time. For such values, the optimal pattern is a very low concentration at an earlier time and a peak concentration at a later time.

³Because the exact energetic cost diverges to ∞ for $u \rightarrow u^{\min}$, $u(t)$ is truncated at u^{zf} (the concentration lower than u^{zf} is

by the quadratic approximation is energetically efficient with the exact definition.

3.2 Slow relaxation of the decoder causes overshooting

We considered the effects of time scale of the decoder on overshooting of the optimal signal. When increasing (decreasing) β_1 or β_2 , the relaxation time of the decoder becomes shorter (longer). We first varied β_2 while keeping other parameters unchanged, except for μ_2^{trg} (the other parameters are the same as those in Fig. 5(a)). Since we are interested in the shape rather than the magnitude, we normalized the signal as follows: $\tilde{u}(t) = u(t)/\sqrt{\tilde{\Pi}}$, which guarantees the unit energy $\tilde{\Pi} = 1$. Figure 5(b) shows the normalized signal $\tilde{u}(t)$ for three cases: $\beta_2 = 0.2$ (solid line), $\beta_2 = 1.0$ (dashed line), and $\beta_2 = 5.0$ (dotted line). As shown above, the overshooting pattern emerges when μ_2^{trg} is close to the saturation value. Thus, for each β_2 value, μ_2^{trg} is set to near the maximal reachable value (parameter details are shown in the caption of Fig 5(b)). When $\beta_2 = 5.0$, the optimal signal does not overshoot, but the other two settings do. From this result, when the relaxation time of X_2 is sufficiently shorter than T , the steep (overshooting) pattern does not minimize energy consumption. The same calculation was performed for β_1 and we found that all of the optimal signals exhibit the overshooting (see the supplementary material). This implies that the relaxation time of X_1 is not responsible for the overshooting pattern.

3.3 Tradeoff between energy and uncertainty

In Fig. 5(c), we next evaluated the dependence on the weight w of the energy $\tilde{\Pi}$ and the uncertainty $\gamma_{i_{\text{out}}}(T)$ for two parameter settings. Parameters of the first setting is the same as those in Fig. 4(b) whose results are plotted by solid (energy) and dotted (uncertainty) lines. The second setting highlights the uncertainty variation when we change w and these results are shown by dashed (energy) and dot-dashed (uncertainty) lines (parameter details are described in the caption of Fig. 5(c)). In Fig. 5(c), we plot the ratio of the energy and uncertainty to those at the minimum weight w^{min} , where w^{min} is the minimum of w for each parameter setting. For the both settings, as w increases, the uncertainty increases, and the energy decreases; there is thus a tradeoff between the energy and the uncertainty, since they cannot be minimized simultaneously. For cellular inference, the tradeoff between uncertainty and energy consumption has been confirmed by several studies [42–45]. Similarly, in biochemical clocks, it has been shown that there is a tradeoff between temporal accuracy and energy consumption [46]. These studies [43–46] calculated the entropy production, which is the energy required for maintaining a system at NESS. There is also a tradeoff between the energy cost and information coding in neural systems ([20] and references therein). We have shown that a similar relation also holds for dynamical signals.

3.4 Calculation with simplified model

We identified that the steep (overshooting) pattern minimizes the energy. Let us explain this mechanism with a simplified two-stage model:

$$\dot{x}_1(t) = u(t), \quad \dot{x}_2(t) = \alpha_2 x_1 - \beta_2 x_2, \quad (17)$$

along with a delta-function stimulus, $u(t) = \delta(t - t_s)$ [t_s is the time of the stimulus, where $0 < t_s < T$]. From Eq. (17), the final output concentration is

$$x_2(T) = \frac{\alpha_2}{\beta_2} \left\{ 1 - e^{-\beta_2(T-t_s)} \right\}. \quad (18)$$

When the relaxation of X_2 is very slow ($\beta_2^{-1} \gg T$), the output concentration is $x_2(T) \simeq \alpha_2(T - t_s)$, which shows that the signal at an earlier time has a greater effect than at a later time; the steep pattern allows the output concentration to reach the target concentration at a lower cost. For the fast relaxation case ($\beta_2^{-1} \ll T$), we obtain $x_2(T) \simeq \alpha_2 \beta_2^{-1}$, which shows that $x_2(T)$ does not depend on t_s ; it is not advantageous for the signal to have a peak at an earlier time. Therefore, when the relaxation time of the decoder is very fast, the steep pattern does not confer advantages for minimizing the energy consumption; this agrees with the identified as u^{zf} .

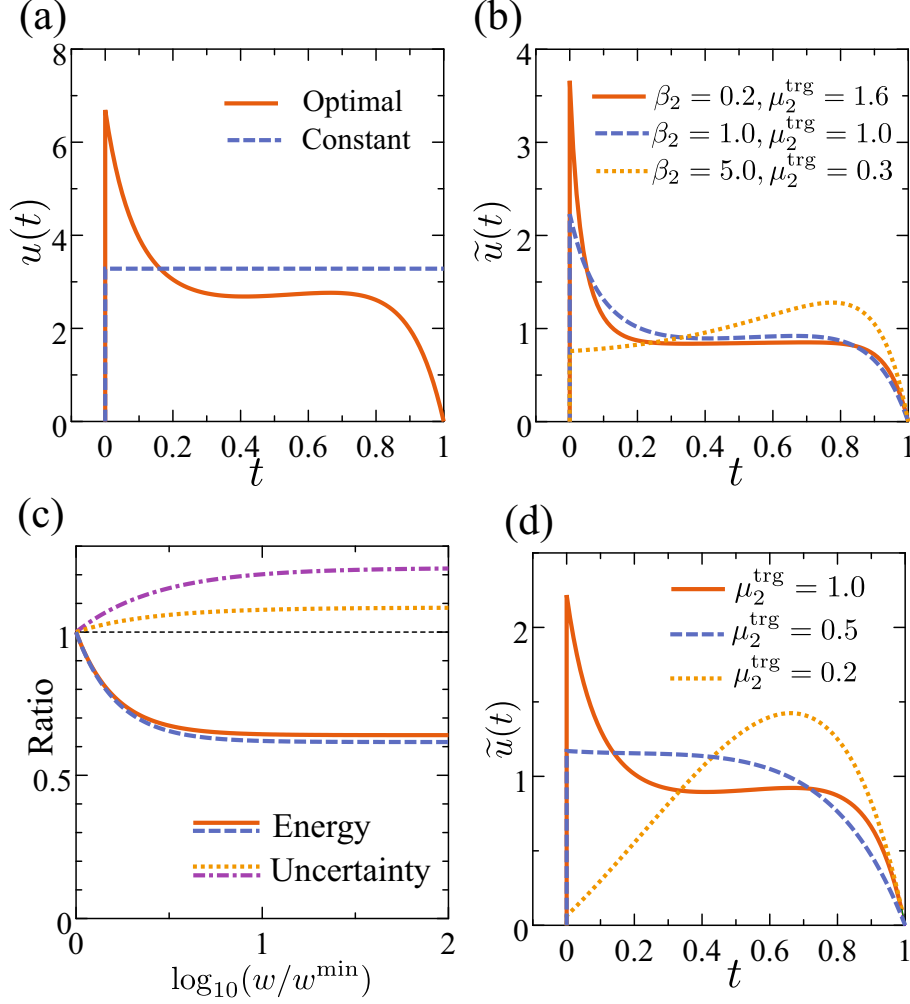


Figure 5: Results of the two-stage model. (a) Comparison of the optimal signal (solid line) and a constant signal (dashed line), which attain the same target concentration $\mu_2^{\text{trg}} = 1.0$ ($w = 1.0$ for the optimal signal). (b) Normalized signal $\tilde{u}(t)$ for three values of β_1 : $\beta_2 = 0.2$ and $\mu_2^{\text{trg}} = 1.6$ (solid line), $\beta_2 = 1.0$ and $\mu_2^{\text{trg}} = 1.0$ (dashed line), and $\beta_2 = 5.0$ and $\mu_2^{\text{trg}} = 0.3$ (dotted line). We set $w = 1.0$. (c) Energy and uncertainty dependence on w for two cases: $\mu_2^{\text{trg}} = 0.2$, $\alpha_1 = 2.0$, $\alpha_2 = 2.0$, $\beta_1 = 1.0$, and $\beta_2 = 1.0$ [parameters are the same as those in Fig. 4(b); solid (energy) and dotted (uncertainty) lines] and $\mu_2^{\text{target}} = 0.5$, $\alpha_1 = 0.5$, $\alpha_2 = 10.0$, $\beta_1 = 0.1$, and $\beta_2 = 0.1$ [dashed (energy) and dot-dashed (uncertainty) lines]. Ranges of w are $1.2 \times 10^{-3} \leq w \leq 1.2 \times 10^{-1}$ for the former and $0.03 \leq w \leq 3.0$ for the latter. We plot the ratio of energy and uncertainty to those at the minimum weight w^{\min} . (d) Variation of the normalized signal $\tilde{u}(t)$ in response to the target concentration μ_2^{trg} for $w = 1.2 \times 10^{-3}$: $\mu_2^{\text{trg}} = 0.2$ (dotted line), 0.5 (dashed line), and 1.0 (solid line). In (a)–(d), the unspecified parameters are the same as those in Fig. 4(a).

optimal control calculation shown in Fig. 5(b). Next, suppose there is only a single stage required to decode the signal $\dot{x}_1(t) = u(t)$, where $x_1(T)$ is the output concentration (a single-stage model). In this case, the final output concentration is $x_1(T) = 1$ and does not depend on t_s , implying that the steep patterns do not minimize the energy. On the other hand, when there is a third stage $\dot{x}_3 = \alpha_3 x_2 - \beta_3 x_3$ in addition to Eqs. (17) (a three-stage model), we find that the final concentration $x_3(T)$ depends on t_s , unless $\beta_2^{-1}, \beta_3^{-1} \ll T$ [for $\beta_2^{-1}, \beta_3^{-1} \gg T$, we have $x_3(T) \simeq \alpha_2 \alpha_3 (T - t_s)^2 / 2$, and for $\beta_2^{-1}, \beta_3^{-1} \ll T$, $x_3(T) = \alpha_2 \alpha_3 / (\beta_2 \beta_3)$]. Thus, the steep patterns generally minimize the energy consumption when the relaxation of the decoder is slow and there are more than two stages in the decoding.

The effect of the gradual pattern can be accounted for by the moment equation. The variance γ_2 and covariance ρ_{12} are governed by (cf. moment equations in the supplementary material)

$$\dot{\gamma}_2(t) = 2(\alpha_2 \rho_{12} - \beta_2 \gamma_2) + 2Q(\alpha_2 \mu_1 + \beta_2 \mu_2), \quad (19)$$

$$\dot{\rho}_{12}(t) = \alpha_2 \gamma_1 - \rho_{12}(\alpha_1 u + \beta_1 + \beta_2). \quad (20)$$

We find that the main reason for the difference between the variance $\gamma_2(T)$ of the steep and gradual patterns is the area $\int_0^T \rho_{12}(t) dt$; namely, a smaller area yields a smaller value for $\gamma_2(T)$. From Eq. (20), because the decay velocity of $\rho_{12}(t)$ depends on u , a higher concentration of u at a later time results in a smaller value for $\rho_{12}(t)$, which corresponds to the gradual pattern of $u(t)$.

4 Discussion and Conclusion

Our result provides insights into experimentally observed dynamical patterns. Reference [8] reported the dynamical pattern of ERK activity in response to different strengths of extracellular stimulus (i.e., the ligand concentration); the pattern is steep when stimulated by a strong stimulus, and it is gradual when stimulated by a weak one. This experimental observation can be accounted for by our model. We show that the optimal signal is steep for larger values of μ_2^{trg} and gradual for smaller values (Fig. 5(d)). It is expected that the strong and weak ligand stimuli result in strong and weak responses, respectively, i.e., higher and lower output concentrations. Therefore, the ERK activity induced by the strong ligand stimulus may be related to $\mu_2^{\text{trg}} = 1.0$, and that induced by the weak one is related to $\mu_2^{\text{trg}} = 0.2$. When the target concentration is higher (i.e., $\mu_2^{\text{trg}} = 1.0$), the magnitude of the signal is larger, and hence the effect of the energy of the signal on the objective function R (Eq. (1)) is greater than that of the variance $\gamma_2(T)$. In contrast, for the smaller values of μ_2^{trg} (i.e., $\mu_2^{\text{trg}} = 0.2$), the variance $\gamma_2(T)$ becomes the leading term because the energy of the signal is smaller. Therefore, the steep pattern is preferable when the target concentration is higher, while the gradual one is preferable when the target concentration is lower. These theoretical results qualitatively agree with the observed dynamical patterns reported in Ref. [8].

Along with conditions for the steep pattern, the overshooting dynamics minimize the energy of the input signals when the total concentration x_1^{tot} is smaller and the target concentration $\mu_{i_{\text{out}}}^{\text{trg}}$ is higher. Surprisingly, this behavior can be found in several dynamical patterns; for example, activities of the ERK, the I κ B kinase (IKK), which regulates the transcription factor NF- κ B, and the kinase AKT show this behavior [4, 39, 47–49]. These examples indicate that the pattern has biological advantages. We also note the biochemical origin of the overshoot. For example, simple incoherent feed-forward loops [1, 2, 50, 51] and activation-deactivation motifs [52] can generate such a pattern, and these motifs can indeed be found in signaling pathways. Furthermore, a strongly damped oscillation is indistinguishable from overshooting. Although NF- κ B is known to exhibit damped oscillation upon stimulation, some studies [53, 54] are skeptical about the functional role of the NF- κ B oscillation; that is, the NF- κ B oscillation may be a by-product of inducing overshooting. Overshooting has often been observed in actual dynamical patterns, but its functional advantage has not been well understood. We have shown that this pattern produces direct benefits.

Acknowledgments

This work was supported by KAKENHI Grant No. 16K00325 from the Ministry of Education, Culture, Sports, Science and Technology.

References

- [1] Alon U 2007 *Nat. Rev. Genet.* **8** 450–461
- [2] Alon U 2007 *An Introduction to Systems Biology* (CRC Press)
- [3] Behar M and Hoffmann A 2010 *Curr. Opin. Genetics Dev.* **20** 684–693
- [4] Kubota H, Noguchi R, Toyoshima Y, Ozaki Y i, Uda S, Watanabe K, Ogawa W and Kuroda S 2012 *Mol. Cell* **46** 820–832
- [5] Purvis J E, Karhohs K W, Mock C, Batchelor E, Loewer A and Lahav G 2012 *Science* **336** 1440–1444
- [6] Purvis J E and Lahav G 2013 *Cell* **152** 945–956
- [7] Sonnen K F and Aulehla A 2014 *Sem. Cell. Dev. Biol.* **34** 91–98
- [8] Selimkhanov J, Taylor B, Yao J, Pilko A, Albeck J, Hoffmann A, Tsimring L and Wollman R 2014 *Science* **346** 1370–1373
- [9] Lin Y, Sohn C H, Dalal C K, Cai L and Elowitz M B 2015 *Nature* **527** 54–58
- [10] Tostevin F and ten Wolde P R 2009 *Phys. Rev. Lett.* **102** 218101
- [11] Mora T and Wingreen N S 2010 *Phys. Rev. Lett.* **104** 248101
- [12] Mugler A, Walczak A M and Wiggins C H 2010 *Phys. Rev. Lett.* **105** 058101
- [13] Hansen A S and O’Shea E K 2013 *Mol. Syst. Biol.* **9** 704
- [14] Kobayashi T J 2010 *Phys. Rev. Lett.* **104** 228104
- [15] Mc Mahon S S, Lenive O, Filippi S and Stumpf M P H 2015 *J. R. Soc. Interface* **12** 20150597
- [16] Becker N B, Mugler A and ten Wolde P R 2015 *Phys. Rev. Lett.* **115** 258103
- [17] Makadia H K, Schwaber J S and Vadigepalli R 2015 *PLoS Comput. Biol.* **11** e1004563
- [18] Tostevin F, de Ronde W and ten Wolde P R 2012 *Phys. Rev. Lett.* **108** 108104
- [19] Laughlin S B 2001 *Curr. Opin. Neurobiol.* **11** 475–480
- [20] Sengupta B and Stemmler M B 2014 *Proc. IEEE* **102** 738–750
- [21] Mehta P, Lang A H and Schwab D J 2016 *J. Stat. Phys.* **162** 1153–1166
- [22] McDonnell M D, Stocks N G, Pearce C E M and Abbott D 2008 *Stochastic resonance* (Cambridge University Press)
- [23] Kamien M I and Schwartz N L 2012 *Dynamic optimization: the calculus of variations and optimal control in economics and management* (Dover Publications)
- [24] Hull D G 2013 *Optimal control theory for applications* (Springer Science & Business Media)
- [25] Gillespie D T 2000 *J. Chem. Phys.* **113** 297–306
- [26] Klipp E, Liebermeister W, Wierling C, Kowald A, Lehrach H and Herwig R 2013 *Systems Biology* (Wiley-Blackwell)
- [27] Forger D B and Paydarfar D 2004 *J. Theor. Biol.* **230** 521–532
- [28] Moehlis J, Shea-Brown E and Rabitz H 2006 *J. Comput. Nonlin. Dyn.* **1** 358–367
- [29] Hasegawa Y and Arita M 2014 *J. R. Soc. Interface* **11** 20131018

- [30] Hasegawa Y and Arita M 2014 *Phys. Rev. Lett.* **113** 108101
- [31] Iolov A, Ditlevsen S and Longtin A 2014 *J. Neural Eng.* **11** 046004
- [32] Rodriguez R and Tuckwell H C 1996 *Phys. Rev. E* **54** 5585–5590
- [33] Tuckwell H C and Jost J 2009 *Physica A* **388** 4115–4125
- [34] Qian H and Beard D A 2005 *Biophys. Chem.* **114** 213–220
- [35] Qian H 2007 *Annu. Rev. Phys. Chem.* **58** 113–142
- [36] Beard D A and Qian H 2008 *Chemical biophysics: quantitative analysis of cellular systems* (Cambridge University Press)
- [37] Aksan Kurnaz I 2004 *Biotechnol. Bioeng.* **88** 890–900
- [38] Thomson T M, Benjamin K R, Bush A, Love T, Pincus D, Resnekov O, Yu R C, Gordon A, Colman-Lerner A, Endy D and Brent R 2011 *Proc. Natl. Acad. Sci. U.S.A.* **108** 20265–20270
- [39] Sasagawa S, Ozaki Y i, Fujita K and Kuroda S 2005 *Nat. Cell. Biol.* **7** 365–373
- [40] Salazar C, Politi A Z and Höfer T 2008 *Biophys. J.* **94** 1203–1215
- [41] Tănase-Nicola S, Warren P B and ten Wolde P R 2006 *Phys. Rev. Lett.* **97** 068102
- [42] Tu Y 2008 *Proc. Natl. Acad. Sci. U.S.A.* **105** 11737–11741
- [43] Mehta P and Schwab D J 2012 *Proc. Natl. Acad. Sci. U.S.A.* **109** 17978–17982
- [44] Lang A H, Fisher C K, Mora T and Mehta P 2014 *Phys. Rev. Lett.* **113** 148103
- [45] Barato A C, Hartich D and Seifert U 2014 *New J. Phys.* **16** 103024
- [46] Cao Y, Wang H, Ouyang Q and Tu Y 2015 *Nat. Phys.* **11** 772–778
- [47] Werner S L, Barken D and Hoffmann A 2005 *Science* **309** 1857–1861
- [48] Werner S L, Kearns J D, Zadorozhnaya V, Lynch C, O’Dea E, Boldin M P, Ma A, Baltimore D and Hoffmann A 2008 *Genes & Development* **22** 2093–2101
- [49] Mathew S, Sundararaj S, Mamiya H and Banerjee I 2014 *Bioinformatics* **30** 2334–2342
- [50] Mangan S and Alon U 2003 *Proc. Natl. Acad. Sci. U.S.A.* **100** 11980–11985
- [51] Mangan S, Itzkovitz S, Zaslaver A and Alon U 2006 *J. Mol. Biol.* **356** 1073–1081
- [52] Behar M and Hoffmann A 2013 *Biophys. J.* **105** 231–241
- [53] Barken D, Wang C J, Kearns J, Cheong R, Hoffmann A and Levchenko A 2005 *Science* **308** 52–52
- [54] Cheong R, Hoffmann A and Levchenko A 2008 *Mol. Syst. Biol.* **4** 192

Supplementary Material for “Optimal Temporal Patterns for Dynamical Cellular Signaling”

Yoshihiko Hasegawa

This supplementary material describes in detail the calculations introduced in the main text. Equation and figure numbers in this section are prefixed with S (e.g., Eq. (S1) or Fig. S1). Numbers without the prefix (e.g., Eq. (1) or Fig. 1) refer to items in the main text.

1 Energetic cost of signal pattern

We derive the energetic cost of signal U with a simple biochemical model. Details of the thermodynamics of biochemical reactions can be found in Refs. [1–3]. U is activated from \bar{U} by the following reaction:



where α_u and β_u are reaction rates. The time evolution of the concentration u and \bar{u} is

$$\frac{d\bar{u}}{dt} = -\frac{du}{dt} = \beta_u u - \alpha_u \bar{u}, \quad (\text{S2})$$

where u and \bar{u} are the concentrations of U and \bar{U} , respectively (the total concentration $u^{\text{tot}} = u + \bar{u}$ does not change with time). As described in the main text, the deactivation reaction is not the reverse reaction of activation. The activation and deactivation of U are mediated by phosphorylation and dephosphorylation, respectively. These reactions are written as (cf. Eq. (6))



where ATP, ADP, and P_i are adenosine triphosphate, adenosine diphosphate, and inorganic phosphate, respectively; and α_a^0 , β_a^0 , α_d , and β_d^0 are reaction rates. According to the mass action kinetics, the time evolution of the concentrations u and \bar{u} are

$$\frac{d\bar{u}}{dt} = -\frac{du}{dt} = \beta_a^0 c_D u - \beta_d^0 c_P \bar{u} + \alpha_d u - \alpha_a^0 c_T \bar{u}, \quad (\text{S5})$$

where c_T , c_D , and c_P are the concentrations of ATP, ADP, and P_i , respectively. When reaction rates (α_a^0 , β_a^0 , α_d , and β_d^0) are held fixed and the system is closed, the system relaxes to an equilibrium state. However, in cellular environments where the system is open, the concentrations of ATP, ADP, and P_i are approximately constant due to external agents, as described in the main text (we denote the cellular concentrations as $c_T = c_T^0$, $c_D = c_D^0$, and $c_P = c_P^0$). Therefore, the system relaxes to a nonequilibrium steady state (NESS). From Eq. (S5), the steady-state concentration u^{ss} is

$$u^{\text{ss}} = \frac{u^{\text{tot}}(\beta_d + \alpha_a)}{\beta_a + \beta_d + \alpha_a + \alpha_d}. \quad (\text{S6})$$

where $\alpha_a = \alpha_a^0 c_T^0$, $\beta_a = \beta_a^0 c_D^0$, and $\beta_d = \beta_d^0 c_P^0$ (note that $\alpha_u = \alpha_a + \beta_d$ and $\beta_u = \alpha_d + \beta_a$). The steady-state net flux (clockwise direction in Fig. 2(d) in the main text) is

$$\mathcal{J}^{\text{ss}} = \frac{u^{\text{tot}}(\alpha_a \alpha_d - \beta_a \beta_d)}{\beta_a + \beta_d + \alpha_a + \alpha_d}. \quad (\text{S7})$$

The free-energy is dissipated along a cycle $\bar{U} \rightarrow U \rightarrow \bar{U}$ (the clockwise direction in Fig. 2(d)). The chemical potential difference of the cycle is

$$\Delta\phi = \Delta\phi_1 + \Delta\phi_2, \quad (\text{S8})$$

where $\Delta\phi_1$ and $\Delta\phi_2$ are chemical potential differences of Eqs. (S3) and (S4), respectively:

$$\Delta\phi_1 = \Delta\phi_1^0 + k_B\mathcal{T} \ln\left(\frac{uc_D^0}{\bar{u}c_T^0}\right), \quad \Delta\phi_2 = \Delta\phi_2^0 + k_B\mathcal{T} \ln\left(\frac{\bar{u}c_P^0}{u}\right), \quad (\text{S9})$$

where $\Delta\phi_1^0$ and $\Delta\phi_2^0$ are the chemical potentials of the standard state, k_B is the Boltzmann constant, and \mathcal{T} is the temperature. Because each of the chemical potential differences is zero at equilibrium, that is $\Delta\phi_1 = \Delta\phi_2 = 0$, we obtain

$$\Delta\phi_1^0 = -k_B\mathcal{T} \ln\left(\frac{u^{\text{eq}}c_D^{\text{eq}}}{\bar{u}^{\text{eq}}c_T^{\text{eq}}}\right), \quad \Delta\phi_2^0 = -k_B\mathcal{T} \ln\left(\frac{\bar{u}^{\text{eq}}c_P^{\text{eq}}}{u^{\text{eq}}}\right), \quad (\text{S10})$$

where the superscript ‘‘eq’’ denotes the concentration at equilibrium. Furthermore, the net flux \mathcal{J} vanishes at equilibrium (detailed balance), which yields the following condition:

$$\alpha_a^0\alpha_d c_T^{\text{eq}} - \beta_a^0\beta_d c_D^{\text{eq}}c_P^{\text{eq}} = 0. \quad (\text{S11})$$

From Eqs. (S10) and (S11), the free energy dissipation of a single cycle (Eq. (S8)) is

$$\Delta\phi = k_B\mathcal{T} \ln\left(\frac{\beta_a^0\beta_d^0 c_D^0 c_P^0}{\alpha_a^0\alpha_d c_T^0}\right) = k_B\mathcal{T} \ln\left(\frac{\beta_a\beta_d}{\alpha_a\alpha_d}\right). \quad (\text{S12})$$

From Eqs. (S7) and (S12), the instantaneous free energy dissipation \mathcal{P} (i.e. power), which is an analogue of [power] = [current] \times [volage] of electric circuits, is

$$\mathcal{P} = -\mathcal{J}^{\text{ss}}\Delta\phi = k_B\mathcal{T} \frac{u^{\text{tot}}(\alpha_a\alpha_d - \beta_a\beta_d)}{\beta_a + \beta_d + \alpha_a + \alpha_d} \ln\left(\frac{\alpha_a\alpha_d}{\beta_a\beta_d}\right). \quad (\text{S13})$$

From Eq. (S13), the energy dissipated during the period $0 \leq t \leq T$ is

$$\Pi = \int_0^T \mathcal{P} dt. \quad (\text{S14})$$

We assume that kinase activity is controlled by an upstream molecular species and thus α_a^0 (i.e. α_a) varies temporally. When relaxation of the system to NESS is sufficiently fast [i.e., $1/(\beta_a + \beta_d + \alpha_a + \alpha_d) \ll T$], the concentration u is well approximated by u^{ss} for the time-varying case. From Eq. (S6), we can write α_a in terms of u as follows:

$$\alpha_a = \frac{u}{u^{\text{tot}} - u} (\alpha_d + \beta_a) - \beta_d. \quad (\text{S15})$$

Because $\alpha_a > 0$, u must satisfy $u > u^{\text{min}}$, where

$$u^{\text{min}} = \frac{u^{\text{tot}}\beta_d}{\beta_a + \beta_d + \alpha_d}. \quad (\text{S16})$$

Because it is numerically difficult to use Eq. (S13) in the optimal control calculations, we approximate the power \mathcal{P} with a simple equation. $\mathcal{P} = 0$ at a zero-flux point $u = u^{\text{zf}}$ with

$$u^{\text{zf}} = \frac{u^{\text{tot}}\beta_d}{\beta_d + \alpha_d}, \quad (\text{S17})$$

where \mathcal{J} vanishes (note that $u^{\text{zf}} > u^{\text{min}}$ always holds). Assuming that u^{zf} is sufficiently small (which may be approximated as 0), $\mathcal{P} = 0$ when u is very low concentration. Furthermore, \mathcal{P} increases superlinearly as u increases from $u = u^{\text{zf}}$. Also the approximation needs to be computationally feasible for the optimal control. Taking into account the above requirements, we may approximate $\mathcal{P} \simeq \tilde{\mathcal{P}}$ with

$$\tilde{\mathcal{P}} = qu^2, \quad (\text{S18})$$

where $q > 0$ is a proportionality coefficient. From Eq. (S18), we represent the energy of the signal as

$$\tilde{\Pi} = \int_0^T \tilde{\mathcal{P}} dt = \int_0^T qu(t)^2 dt.$$

In the main calculation, we employ $q = 1$, because the scaling of q is offset by the weight parameter w in the performance index (cf. Eq. (1)).

2 Moment equation

In this section, we derive the equations that must be satisfied by the mean, variance, and covariance. We consider the Fokker–Planck equation (FPE):

$$\frac{\partial}{\partial t}P(\mathbf{x};t) = -\sum_{i=1}^N \frac{\partial}{\partial x_i}F_i(\mathbf{x};t)P(\mathbf{x};t) + \sum_{i=1}^N \frac{\partial^2}{\partial x_i^2}G_i(\mathbf{x};t)P(\mathbf{x};t), \quad (\text{S19})$$

where $\mathbf{x} = (x_1, x_2, \dots, x_N)$, $P(\mathbf{x};t)$ is the probability density of \mathbf{x} at time t , and $F_i(\mathbf{x};t)$ and $G_i(\mathbf{x};t)$ are the drift and diffusion terms, respectively (we do not consider cross terms, such as $\partial^2/\partial x_i \partial x_j$ ($i \neq j$), as these terms do not emerge in our model). We denote the range of x_i as $x_i^{\min} \leq x_i \leq x_i^{\max}$; for example, in the two-stage model, $x_1^{\min} = 0$ and $x_1^{\max} = x_1^{\text{tot}}$ for X_1 . Because the concentration must satisfy these constraints, we impose reflecting walls at the boundaries. Writing the FPE (S19) as the continuity equation, we have

$$\frac{\partial}{\partial t}P(\mathbf{x};t) + \sum_{i=1}^N \frac{\partial}{\partial x_i}J_i(\mathbf{x};t) = 0, \quad (\text{S20})$$

where J_i denotes the probability current:

$$J_i(\mathbf{x};t) = F_i(\mathbf{x};t)P(\mathbf{x};t) - \frac{\partial}{\partial x_i}G_i(\mathbf{x};t)P(\mathbf{x};t). \quad (\text{S21})$$

Due to the reflecting walls, the current vanishes at the boundaries, i.e.,

$$J_i(\mathbf{x};t) = 0 \quad \text{at} \quad x_i = x_i^{\min} \text{ and } x_i = x_i^{\max}. \quad (\text{S22})$$

Here, we consider the (uncentralized) moment ($k \neq \ell$):

$$\langle x_k^m x_\ell^n \rangle = \int d\mathbf{x} x_k^m x_\ell^n P(\mathbf{x};t), \quad (\text{S23})$$

where

$$\int d\mathbf{x} = \int_{x_1^{\min}}^{x_1^{\max}} dx_1 \int_{x_2^{\min}}^{x_2^{\max}} dx_2 \cdots \int_{x_N^{\min}}^{x_N^{\max}} dx_N.$$

The time evolution of the moment obeys

$$\begin{aligned} \frac{d}{dt} \langle x_k^m x_\ell^n \rangle &= \int d\mathbf{x} x_k^m x_\ell^n \frac{\partial}{\partial t}P(\mathbf{x};t), \\ &= \sum_{i=1}^N \int d\mathbf{x} x_k^m x_\ell^n \left[-\frac{\partial}{\partial x_i}F_i(\mathbf{x};t)P(\mathbf{x};t) + \frac{\partial^2}{\partial x_i^2}G_i(\mathbf{x};t)P(\mathbf{x};t) \right] d\mathbf{x}, \end{aligned} \quad (\text{S24})$$

where Eq. (S19) is used. Using integration by parts, we have

$$\begin{aligned} \frac{d}{dt} \langle x_k^m x_\ell^n \rangle &= -\sum_{i=1}^N \int d\mathbf{x}_{-i} \left\{ x_k^m x_\ell^n J_i(\mathbf{x};t) \right\} \Big|_{x_i^{\min}}^{x_i^{\max}} \\ &+ \sum_{i=1}^N \int d\mathbf{x} \left[\frac{\partial (x_k^m x_\ell^n)}{\partial x_i} F_i(\mathbf{x};t)P(\mathbf{x};t) - \frac{\partial (x_k^m x_\ell^n)}{\partial x_i} \frac{\partial}{\partial x_i} G_i(\mathbf{x};t)P(\mathbf{x};t) \right], \end{aligned} \quad (\text{S25})$$

where we formally define

$$\int d\mathbf{x}_{-i} = \prod_{j=1, j \neq i}^N \int_{x_j^{\min}}^{x_j^{\max}} dx_j.$$

From Eq. (S22), the first term in Eq. (S25) vanishes, and we obtain

$$\begin{aligned} \frac{d}{dt} \langle x_k^m x_\ell^n \rangle &= \sum_{i=1}^N \int d\mathbf{x} \frac{\partial (x_k^m x_\ell^n)}{\partial x_i} F_i(\mathbf{x};t)P(\mathbf{x};t) \\ &+ \sum_{i=1}^N \int d\mathbf{x}_{-i} \left[-\frac{\partial (x_k^m x_\ell^n)}{\partial x_i} G_i(\mathbf{x};t)P(\mathbf{x};t) \Big|_{x_i^{\min}}^{x_i^{\max}} + \int dx_i \frac{\partial^2 (x_k^m x_\ell^n)}{\partial x_i^2} G_i(\mathbf{x};t)P(\mathbf{x};t) \right], \end{aligned}$$

where we again used integration by parts. If we assume that $G_i(\mathbf{x}; t)P(\mathbf{x}; t)$ is negligible at the boundaries $x_i = x_i^{\min}$ and $x_i = x_i^{\max}$, we have

$$\frac{d}{dt} \langle x_k^m x_\ell^n \rangle = \sum_{i=1}^N \left[\left\langle \frac{\partial (x_k^m x_\ell^n)}{\partial x_i} F_i(\mathbf{x}; t) \right\rangle + \left\langle \frac{\partial^2 (x_k^m x_\ell^n)}{\partial x_i^2} G_i(\mathbf{x}; t) \right\rangle \right]. \quad (\text{S26})$$

Equation (S26) is an equation for uncentralized moments. In order to obtain closed equations for the mean, variance, and covariance for general $F_i(\mathbf{x}; t)$ and $G_i(\mathbf{x}; t)$, we expand x_i around the mean values as $x_i - \mu_i = \delta x_i$, with $\mu_i = \langle x_i \rangle$. Retaining terms up to the second order, such as $\langle \delta x_k^m \delta x_\ell^n \rangle$ with $m + n = 2$, we obtain closed equations with respect to $\mu_i(t)$, $\gamma_i(t) = \langle (x_i(t) - \mu_i(t))^2 \rangle$, and $\rho_{ij} = \langle (x_i - \mu_i)(x_j - \mu_j) \rangle$. However note that in the two-stage model, because $F_i(\mathbf{x}; t)$ and $G_i(\mathbf{x}; t)$ are linear with respect to \mathbf{x} , we can obtain closed differential equations for $\mu_i(t)$, $\gamma_i(t)$, and $\rho_{ij}(t)$ without the truncation.

3 Differential equations of optimal control

Deterministic equations for the two-stage model are given by Eqs. (15) and (16). From Eq. (3), the corresponding FPE is

$$\begin{aligned} \frac{\partial}{\partial t} P(\mathbf{x}; t) = & \left[-\frac{\partial}{\partial x_1} \{ \alpha_1 u(x_1^{\text{tot}} - x_1) - \beta_1 x_1 \} - \frac{\partial}{\partial x_2} \{ \alpha_2 x_1 - \beta_2 x_2 \} \right. \\ & \left. + Q \frac{\partial^2}{\partial x_1^2} \{ \alpha_1 u(x_1^{\text{tot}} - x_1) + \beta_1 x_1 \} + Q \frac{\partial^2}{\partial x_2^2} \{ \alpha_2 x_1 + \beta_2 x_2 \} \right] P(\mathbf{x}; t). \end{aligned} \quad (\text{S27})$$

From Eq. (S26), the moment equations are

$$\dot{\mu}_1 = \alpha_1 u(x_1^{\text{tot}} - \mu_1) - \beta_1 \mu_1, \quad (\text{S28})$$

$$\dot{\mu}_2 = \alpha_2 \mu_1 - \beta_2 \mu_2, \quad (\text{S29})$$

$$\dot{\gamma}_1 = 2Q \{ \beta_1 \mu_1 + \alpha_1 u(x_1^{\text{tot}} - \mu_1) \} - 2\gamma_1 (\alpha_1 u + \beta_1), \quad (\text{S30})$$

$$\dot{\gamma}_2 = 2(\alpha_2 \rho_{12} - \beta_2 \gamma_2) + 2Q(\alpha_2 \mu_1 + \beta_2 \mu_2), \quad (\text{S31})$$

$$\dot{\rho}_{12} = \alpha_2 \gamma_1 - \rho_{12}(\alpha_1 u + \beta_1 + \beta_2). \quad (\text{S32})$$

Differential equations for the Lagrange multiplier λ_i are obtained from Eq. (13), as follows:

$$\dot{\lambda}_1 = -\alpha_2 \lambda_2 - 2\lambda_3 Q(\beta_1 - \alpha_1 u) - 2\alpha_2 \lambda_4 Q + \lambda_1(\alpha_1 u + \beta_1), \quad (\text{S33})$$

$$\dot{\lambda}_2 = \beta_2 \lambda_2 - 2\beta_2 \lambda_4 Q, \quad (\text{S34})$$

$$\dot{\lambda}_3 = -\alpha_2 \lambda_5 + 2\lambda_3(\alpha_1 u + \beta_1), \quad (\text{S35})$$

$$\dot{\lambda}_4 = 2\beta_2 \lambda_4, \quad (\text{S36})$$

$$\dot{\lambda}_5 = -2\alpha_2 \lambda_4 + \lambda_5(\beta_1 + \beta_2 + \alpha_1 u). \quad (\text{S37})$$

Here, $u(t)$ is obtained from Eq. (14):

$$u(t) = \frac{\alpha_1}{2wq} (2Q\lambda_3\mu_1 - 2Q\lambda_3x_1^{\text{tot}} + \rho_{12}\lambda_5 + 2\gamma_1\lambda_3 + \lambda_1\mu_1 - \lambda_1x_1^{\text{tot}}). \quad (\text{S38})$$

According to the optimal control theory [4], boundary conditions of $\mathbf{z} = (\mu_1, \mu_2, \gamma_1, \gamma_2, \rho_{12})$ and $\boldsymbol{\lambda}$ are as follows: $\mu_1(0) = 0$, $\mu_2(0) = 0$, $\gamma_1(0) = 0$, $\gamma_2(0) = 0$, $\rho_{12}(0) = 0$, $\mu_2(T) = \mu_2^{\text{trg}}$, $\lambda_1(T) = 0$, $\lambda_3(T) = 0$, $\lambda_4(T) = 1$, and $\lambda_5(T) = 0$. We numerically solved this two-point boundary value problem with a `bvp4c` function in *Matlab*.

4 Optimal signal dependence on β_1

In the main text, we studied shape of the optimal signal dependence on β_2 (Section 3.2). We performed the same calculation for β_1 , i.e. β_1 and μ_2^{trg} are varied while keeping other parameters unchanged (the other parameters are the same as those in Fig. 4(a)). Figure S1 shows normalized signal $\tilde{u}(t) = u(t)/\sqrt{\Pi}$ for three cases: $\beta_1 = 0.2$ and $\mu_2^{\text{trg}} = 1.1$ (solid line), $\beta_1 = 1.0$ and $\mu_2^{\text{trg}} = 1.0$ (dashed line), and $\beta_1 = 5.0$ and $\mu_2^{\text{trg}} = 0.9$ (dotted line). We found that all the optimal signals exhibit the overshooting. This implies that the relaxation time of X_1 is not responsible for the overshooting pattern.

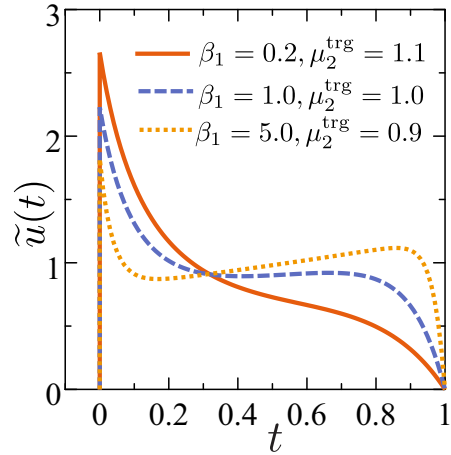


Figure S1: Normalized signal $\tilde{u}(t)$ for three values of β_1 : $\beta_1 = 0.2$ and $\mu_2^{\text{trg}} = 1.1$ (solid line), $\beta_1 = 1.0$ and $\mu_2^{\text{trg}} = 1.0$ (dashed line), and $\beta_1 = 5.0$ and $\mu_2^{\text{trg}} = 0.9$ (dotted line). We set $w = 1.0$ and the unspecified parameters are the same as those in Fig. 4(a).

References

- [1] Qian H and Beard D A 2005 *Biophys. Chem.* **114** 213–220
- [2] Qian H 2007 *Annu. Rev. Phys. Chem.* **58** 113–142
- [3] Beard D A and Qian H 2008 *Chemical biophysics: quantitative analysis of cellular systems* (Cambridge University Press)
- [4] Hull D G 2013 *Optimal control theory for applications* (Springer Science & Business Media)